


Electronic, magnetic properties and pressure-induced phase transition of new D0₁₉ Fe₂MnSn Heusler alloy

I. Bouhamou, H. Abbassa, C. Abbas, A. Boukortt, E.H. Abbas  , A. Benbedra

Abdelhamid Ibn Badis University-Mostaganem, Mostaganem, Algeria

 habib.abbes.etu@univ-mosta.dz

Abstract. Using ab-initio calculations based on density functional theory (DFT) with the generalized gradient approximation (GGA), structural, electronic and magnetic properties of Fe₂MnSn full Heusler alloy are calculated within the framework to describe the effect of hydrostatic stress. The total system energy optimization indicates that the ground state corresponds to the hexagonal (D0₁₉) structure in ferromagnetic (FM) state. The compound undergoes a structural stress-induced phase transitions under pressure of 7 GPa. The total magnetic moment at the optimized lattice parameters is found 7.19 μ_B , which does not follow the Slater-Pauling rule. The material tends to rapidly lose its spin polarization under 10 GPa hydrostatic stress.

Keywords: Full Heusler; electronic; magnetic; FP-LAPW calculations

Acknowledgements. This work is supported by the Algerian national research projects, PRFU/DGRSDT/MESRS-Algeria (project N° B00L02UN270120220001).

Citation: Bouhamou I, Abbassa H, Abbas C, Boukortt A, Abbas EH, Benbedra A. Electronic, Magnetic Properties and Pressure-induced Phase Transition of New D0₁₉ Fe₂MnSn Heusler Alloy. *Materials Physics and Mechanics*. 2023;51(6): 65-75. DOI: 10.18149/MPM.5162023_6.

Introduction

The search for new materials with specific physical properties is a major challenge for today's industry, depending on the field of application considered (spintronics, energy, materials, ...). In our era, simulation makes possible to explore various properties in the quantum domain such as the structural, electronic and even dynamic properties of matter, often far from any experimental knowledge of the system studied. Ab-initio methods currently have the ability to perform calculations with great precision for different quantities [1–16], such as elasticity, optical spectra, lattice vibration frequencies, etc. Today, spin electronics is looking for new materials and technological challenges that condition the realization of new devices. In many study subjects, Heusler alloys attract the interest of physicists of solid-state for their remarkable physical and magnetic properties, which are frequently encountered [17,18]. More than 3000 Heusler compounds have been discovered to be used in many fields [19] such as the domain of electronic and magnetic technologies (giant magnetoresistance (GMR) [20,21], tunnel magnetoresistance (TMR) [22], and others). It is a family of materials that affects several fields of application such as spintronic [23], superconductivity [24], shape memory alloys (SMA) [25,26] and other fields. The first prototype of Heusler alloy was discovered by Heusler Friedrich in 1903 [27], where it was possible to make magnetic alloys from non-magnetic components. Later, its crystal structure was determined by Bradley and Rodgers in 1934 [28].

Heusler alloys were classified as ternary ferromagnetic compounds with the chemical formula X_2YZ [29,30] where X and Y are transition metals and Z the main group element. Where X atoms occupy the Wyckoff positions $(1/4,1/4,1/4)$ and $(3/4,3/4,3/4)$ while the Y and Z atoms are in positions $(1/2,1/2,1/2)$ and $(0,0,0)$ respectively, in the cubic structure with the space group $Fm\bar{3}m$ (SG 225) according the prototype Cu_2MnAl , often noted $(L2_1)$ [31,32].

This crystallographic structure can be sometimes distorted to a tetragonal structure (D_{022}) [33] under the band Jahn-Teller effect. Another cubic structure is often observed in these alloys, known us the inverse structure (noted XA) where X atoms are located in different environments. Recently, a new hexagonal structure has been confirmed as the ground state structure for some Heusler alloys, this crystallographic structure (D_{019}) has been derived from the Ni_3Sn prototype structure with the space group $P6_3/mmc$ [34], where the chemical formula X_3Z is transformed to X_2YZ , by the substitution of one of X atoms with another transition metals Y. Non-cubic Heusler compounds used Fe_2MnSn may exhibit large magneto crystalline anisotropy [35], which gives them a special importance, it is a necessary condition for hard magnetic applications [36,37]. Motivating by this property, we have investigated the hexagonal D_{022} Heusler alloy Fe_2MnSn , which shows a high total magnetic moment (about $7 \mu_B/f.u.$). The studied compound was synthesized experimentally [35], we note that our theoretical calculations showed that both cubic and hexagonal phases of Fe_2MnSn Heusler alloy are energetically very close.

In the present work, we focus our study on both electronic and magnetic properties of the Fe_2MnSn full-Heusler compound. In addition, we carry out a detailed study about the pressure induced phase transition of the new D_{019} structure (Fig. 1), and we discuss the anomalies of this specific Heusler material.

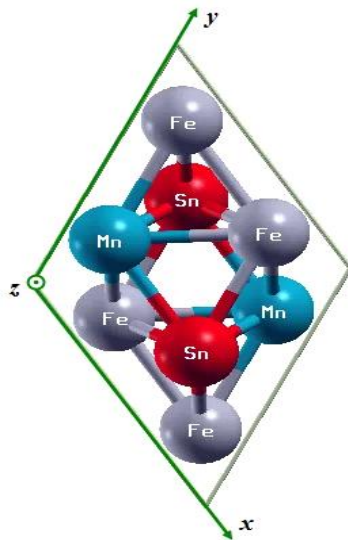


Fig. 1. D_{019} structure for Fe_2MnSn full-Heusler alloy

Computational method

In this study, electronic and magnetic structures calculations were performed using the FP-LAPW method (self-consistent full-potential linearized augmented plane wave) [38,39], this method was integrated into the WIEN2K code simulation [40,41] within the DFT (density functional theory) [42]. For the exchange-correlation correction, it used the GGA-PBE approximation (generalized gradient approximation) depending on the Perdewe-Burkee-Ernzerhof model [43,44] and the GGA-mBJ [45], where the space is divided into the non-overlapping muffin-tin spheres (MT), separated by an interstitial region. For these spheres, basis functions are expanded into spherical harmonic functions, while Fourier series are

expanded for the interstitial area. In our study, muffin-tin sphere radii are 2.10 a.u. for Mn and Fe, 2.25 a.u. for Sn. The convergence of the basis was controlled by $R_{MT}K_{max} = 9$ (cutoff parameter), where the R_{MT} is the smallest of the MT sphere radii, while K_{max} present the largest reciprocal lattice vector used in the plane wave expansion. The G_{max} parameter (magnitude of the most significant vector in charge density Fourier expansion) was 12. The cutoff energy (the separation of valence and core states) was chosen as -6 Ry. Energy test convergence was selected as 0.0001 Ry during self-consistency cycles. For the Brillouin zone integration (BZ), we used the tetrahedron method [40] with 104 particular k points (for cubic structure), and 180 k points (for hexagonal structure) in the irreducible wedge (3000 k-points in all Brillouin zone) in order to construct the charge density in each self-consistency step.

Results and Discussion

Structural Properties. From the first principle calculation based on the density function theory with the generalized gradient approximation, the structural properties of Fe₂MnSn Heusler alloy are calculated in order to well understand the ground state properties. Basing on the structural part, we can predict the other properties (electronic, magnetic, etc.). The structural parameters have always been determined by minimizing the total energy, in this procedure, we calculated and plotted the total energies versus volume for the cubic structure in both XA and L₂₁ prototype and for the Hexagonal D0₁₉ structure in Fig. 2, where we took into consideration the ferromagnetic (FM) and non-magnetic (NM) orders. The structural analysis in Fig. 2 shows that the D0₁₉ (SG: 194) structure in the ferromagnetic state makes the ground state (i.e., the structure more stable) for the Fe₂MnSn compound. In order to determine the fundamental equilibrium parameters, we used the empirical Murnaghan equation of states (1) (E-O-S) [46]:

$$E(V) = \frac{B_0 V}{B'(B' - 1)} \left[\left(\frac{V_0}{V} \right)^{B'} + B' \left(1 - \frac{V_0}{V} \right) - 1 \right] + E_0, \quad (1)$$

where V_0 is the unit cell volume of the ground state, B the bulk modulus and B' its first pressure derivative.

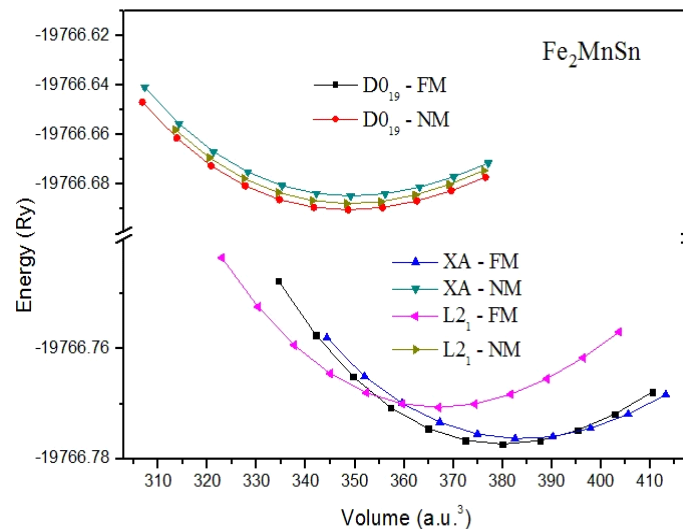


Fig. 2. Total energies vs. volume for Fe₂MnSn Heusler alloy: cubic structures (XA and L₂₁) and D0₁₉ for non-magnetic (NM) and ferromagnetic (FM) states

Obtained results are listed in Table 1, where a and c are the equilibrium lattice parameters, and E_0 the energy of the ground state for each structure, in which the results of the other available calculations are also indicated. It is clear that our results are in good agreement with the others found in literature.

Table 1. Structural parameters, the lattice parameters a and c , Bulk modulus B and its first pressure derivative B' and system energy E_0 for Fe₂MnSn full-Heusler alloy in cubic and hexagonal structures

Structure		a, Å	c, Å	B ₀ , GPa	B'	E ₀ (Ry), eV
Cubic (XA)	This work	6.104		114.15	3.15	-19766.77636
	Ref.[47]	6.084		110.47	6.08	-19766.69924
Cubic (L2 ₁)	This work	6.014		125.92	3.30	-19766.77067
	Ref.[47]	5.958		178.15	5.23	-19766.69677
	Ref.[35]	6.027				
	Ref.[48]	6.010		123		-19766.6946
Hexagonal (D0 ₁₉)	This work	5.419	4.422	129.45	3.84	-19766.77734
	Ref.[35]	5.389	4.310			

Magnetic properties. To describe the magnetic moment, we take into consideration the spin magnetic moment, defined by the deference between the total occupancy of the majority spin and the total occupancy of the minority spin.

The calculated total and local magnetic moments for Fe₂MnSn Heusler alloy are listed in Table 2. We can see that the values μ_B obtained for the three structures studied (XA, L2₁ and D0₁₉) presents a remarkable anomaly between the theoretical and experimental work carried out on this material. For full Heusler X₂YZ alloys, the magnetization M and the number of valence electrons Z are related either by: $M = Z - 18$, $M = Z - 24$, or by $M = Z - 28$ [49–54]. All the results obtained, indicates that this specific compound does not follow any rule among these three rules, it is one of the few Heusler materials that has this particularity.

Table 2. Total and local magnetic moments per formula unit in (μ_B) for Fe₂MnSn full-Heusler alloy

Structure		Total	Fe (1)	Fe (2)	Mn	Sn	Interstitial
Cubic (XA)	This work (GGA)	7.65	2.25	2.54	2.93	-0.06	-0.01
	(mBJ)	7.66					
	Ref. [47]	8.33	2.47	2.67	3.30	-0.06	-0.05
Cubic (L2 ₁)	This work (GGA)	5.81	1.77	1.77	2.41	-0.06	-0.08
	(mBJ)	5.83					
	Ref. [47]	3.00	-0.20	- 0.17	3.37	-0.01	0.01
	Ref. [35]	6.04	1.83	1.83	2.57	-0.14	
	Ref. [48]	5.73	3.47	3.47	2.45	-0.07	
Hexagonal (D0 ₁₉)	This work (GGA)	7.19	2.23	2.23	2.79	-0.09	0.03
	(mBJ)	7.19					
	Ref. [35]	6.50	2.3	2.3	2.3	-0.15	

In our study, the calculated total magnetic moment M_{tot} for the ground state structure (D0₁₉) was found to be 7.19 μ_B . This non-integer value also indicates a metallic ferromagnetic behavior.

Electronic properties. The electronic properties (band structures, densities of states) depend essentially on the distribution of electrons in both valence and conduction bands, as well as on the value of the energy gap. In which, we can analyze and understand the nature of the bonds formed between the different elements of the material, in order to have a better understanding of its behavior.

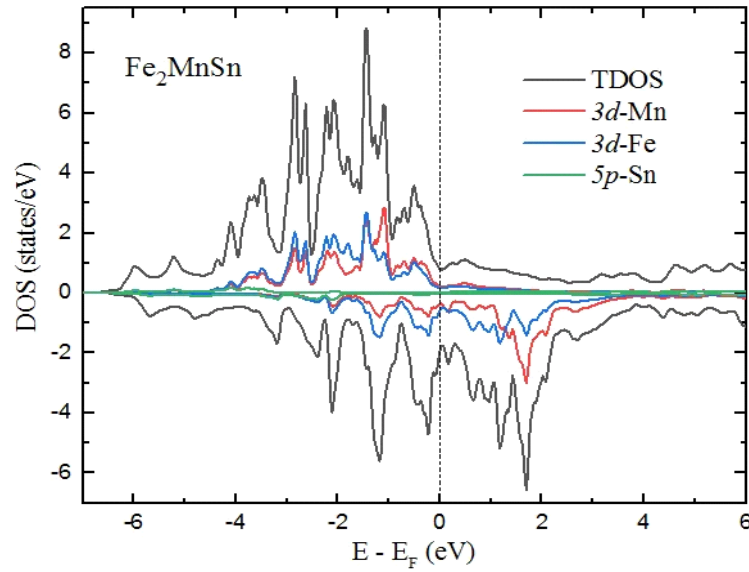


Fig. 3. The calculated total/atomic projected densities of states for Fe₂MnSn Heusler alloy in hexagonal D0₁₉ structure at the ground state

In this subsection, the calculation of the electronic properties such as total/partial densities of states and band structures are shown in Figs. 3 and 4, respectively. The calculations have been made for the equilibrium lattice parameter of the ground state (D0₁₉ structure).

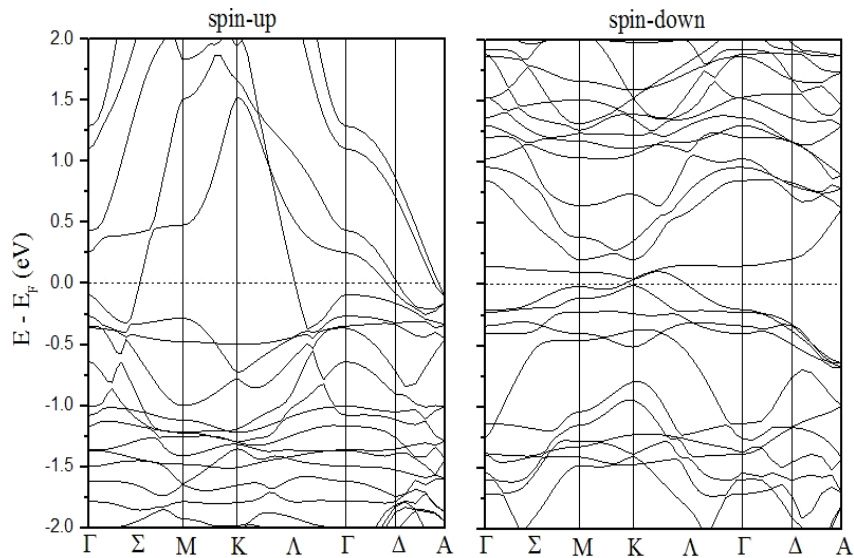


Fig. 4. The calculated band structures for Fe₂MnSn Heusler alloy in hexagonal D0₁₉ structure with both spin-up and spin-down electrons

From Fig. 3, we can see that the density of state of the majority spin-up and minority spin-down electrons show metallic intersections at the Fermi level (E_F), which indicates a metallic character for the studied compound. Below Fermi level, Mn atoms have a major contribution in the total density of states (DOS) for majority spin-up, due to the $3d$ -Mn electrons, while the DOS of the minority spin-down is dominated by $3d$ -Fe electrons. Above Fermi level, Mn atoms dominate both densities of states (spin-up and spin-down). Around Fermi level, the contributions of Mn and Fe atoms are almost identical. Unlike the D0₁₉ structure, the cubic structure has a gap energy. In Table 3, we give the obtained results for the gap energy, using both GGA and mBJ approximations.

Table 3. Gap energy and spin polarisation for Fe₂MnSn full-Heusler alloy

Structure		E _g , eV	
		GGA	mBJ
Cubic (XA)	This work	0.14	0.16
	Ref.[47]	0.16	
Cubic (L2 ₁)	This work	0.30	0.35
	Ref.[47]	0.29	
	Ref.[35]	0.36	
	Ref.[48]	0.35	
Hexagonal (D0 ₁₉)	This work	0	0
	Ref.[35]	0	

According to Fig. 4, the spin-up and spin-down band structures along the points and directions of high symmetry in the first Brillouin zone have metallic intersections at the Fermi level, where no band gap appears around E_F . View of the overlap between the energy bands, this situation also confirms the metallic character of Fe₂MnSn Heusler alloy.

Pressure effect. The second objective in this paper is the study of the effect of hydrostatic pressure on the structural, magnetic and electronic properties, where we chose a range of low pressures (between 0 and 10 GPa). For the structural part, we predicted a phase transition from D0₁₉ hexagonal structure to L2₁ cubic structure, as is shown in Fig. 5. This prediction was made using two methods, the first is based on the structural optimization curves, and is calculating the slope of the common tangent between the two curves (Fig. 5(a)). The second one is based on the calculation of enthalpy variation versus pressure (Fig. 5(b)), where the intersection of the two lines determines the structural transition pressure P_t from hexagonal structure (D0₁₉) to cubic structure (L2₁). The intersection point in Fig. 5(b) indicates the equality of the system enthalpy for both cubic and hexagonal structures, and under the same pressure, 7 GPa. Beyond this critical value, the enthalpy of the cubic structure represents the minimum energy (the line of L2₁ phase passes below that of the D0₁₉ phase), which leads to a structural transition from hexagonal structure to cubic structure. The enthalpy H is given by the following equation:

$$H = E + P.V \quad (2)$$

The two methods present a good coherence and indicate the same value, $P_t = 7$ GPa.

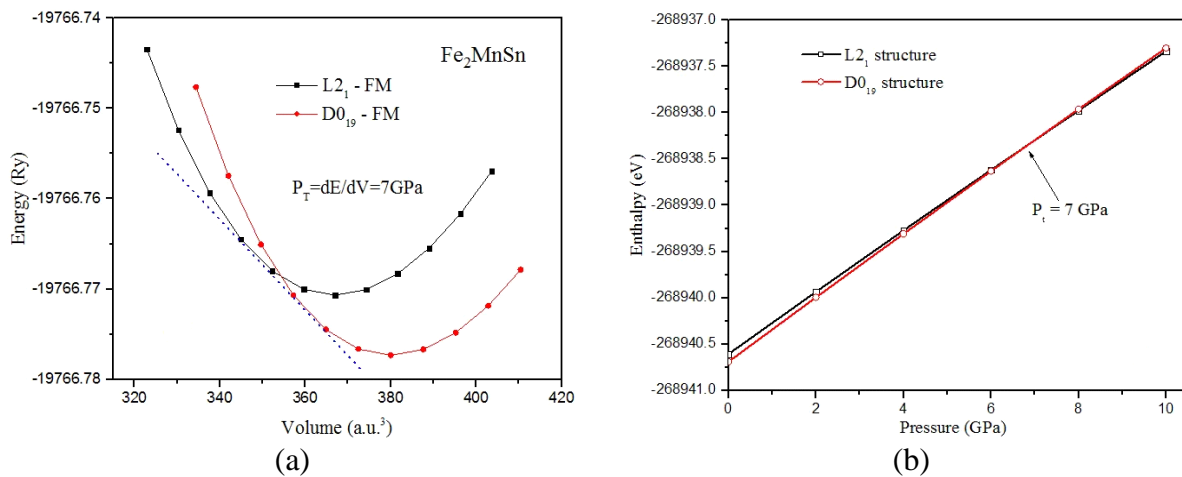


Fig. 5. Structural transition in Fe₂MnSn full-Heusler alloy according to the common slope (a) and the enthalpy variation (b)

We have further studied the effect of pressure on the magnetic and electronic properties for both hexagonal and cubic structures. Figure 6 shows that increasing the pressure reduces the total magnetic moment for the two structures studied, an integer total magnetic moment is found under the effect of the pressures, we found $5.00 \mu_B$ under 6.20 GPa and $7.00 \mu_B$ under 4.78 GPa for the two structures (D0₁₉) and (L2₁) respectively. Generally, an integer total magnetic moment indicates obedience to Slater-Pauling rule and half-metallic character. It is for this purpose that we have calculated and plotted the densities of states of the two structures under the effect of the two pressures indicated in Fig. 7. Contrary to what is expected, the material has another peculiarity, the densities of states present metallic intersections for the two orientations of the spin and for the two structures, then the material keeps its ferromagnetic metallic behavior, and always deviates from Slater-Pauling rule.

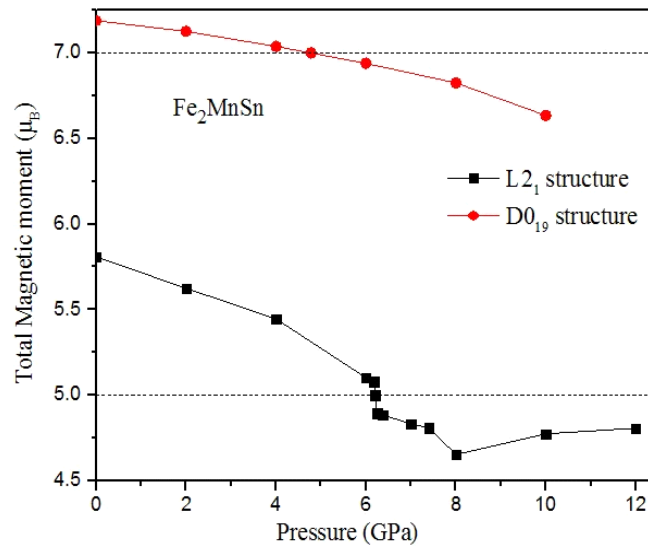


Fig. 6. Total magnetic moment variation as a function of pressure for Fe₂MnSn full-Heusler alloy

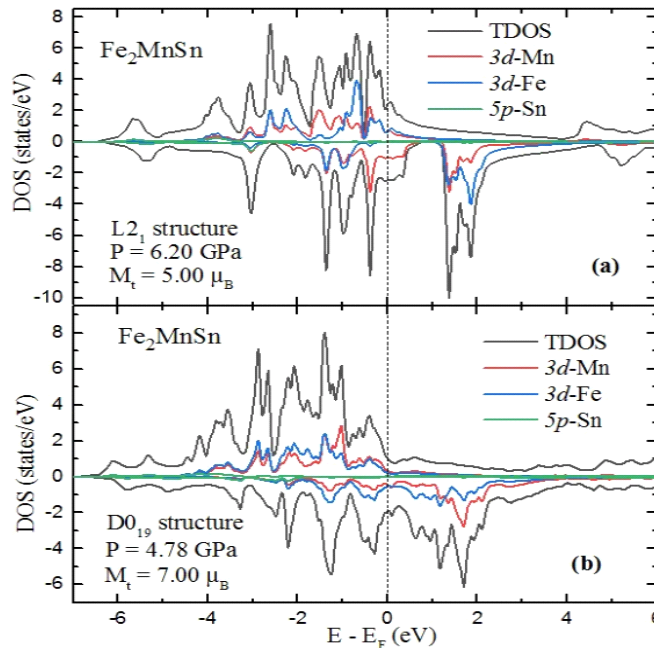


Fig. 7. The calculated total/atomic projected densities of states for Fe₂MnSn Heusler alloy for integer value of total magnetic moment: (a) cubic L₂₁ structure ($5.00 \mu_B$); (b) hexagonal D0₁₉ structure ($7.00 \mu_B$)

To examine the effect of pressure on the metallic character of the material, we calculated and plotted in Fig. 8, the variation of spin polarization versus pressure for the same range and for both hexagonal and cubic structures. We notice that increasing the pressure rapidly decreases the spin polarization for the hexagonal structure ($D0_{19}$), while for the cubic structure ($L2_1$) the variation is slight and alternating.

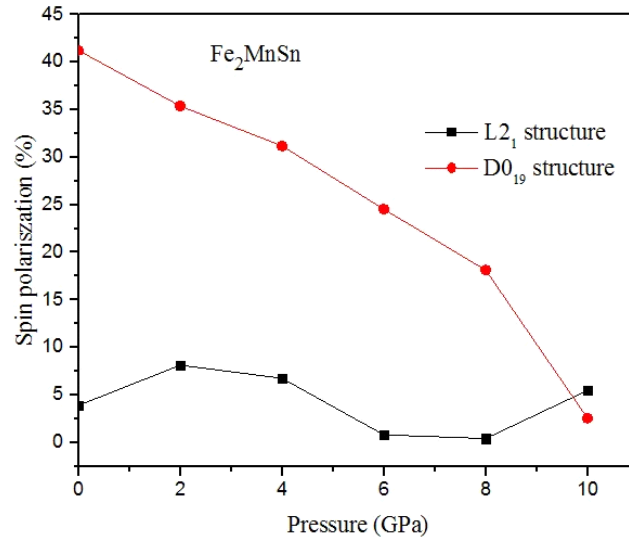


Fig. 8. Spin polarisation variation versus pressure for Fe₂MnSn full-Heusler alloy

Conclusion

In this paper, we have performed a first-principles study of the structural, electronic and magnetic properties, for the ternary full Heusler alloy Fe₂MnSn in the ground state. We also examined the effect of pressure on the evolution of these properties. Our results reveal that the ferromagnetic hexagonal $D0_{19}$ structure makes the ground state for Fe₂MnSn Heusler alloy, and a pressure-induced phase transition (from hexagonal to cubic structure) was predicted under 7 GPa. The study of the electronic band structure and the density of states show that the Fe₂MnSn compound has a metallic character. It retains this character even under the effect of hydrostatic pressure, with a range of 0 to 10 GPa. The total magnetic moment is found 7.19 μ_B , it never follows Slater-Pauling rule, even for an integer total magnetic moment (under pressure). The material tends to rapidly lose its spin polarization under the effect of hydrostatic pressure.

References

1. Ramdane O, Labidi M, Masrou R, Labidi S, Ellouze M, Rehamnia R. Study of Structural, Electronic, and Magnetic Properties of Cubic and Tetragonal Ba₂FeMoO₆. *Journal of Superconductivity and Novel Magnetism*. 2023;36(1): 373–387.
2. Chaabouni R, Ellouze M, Hlil EK, Masrou R, Jotania R. Role of nickel substitution in the structural, magnetic properties, and magnetocaloric effect in La_{0.67}Ba_{0.22}Sr_{0.11}Mn_{0.95}Ni_{0.05}O₃ sample. *Journal of Materials Science: Materials in Electronics*. 2022;33(30): 23524–23541.
3. Kadim G, Masrou R. First-principles investigation of electronic and optical properties of Fe doped in CsBrO₃ for enhanced photocatalytic hydrogen production. *International Journal of Hydrogen Energy*. 2022;47(61): 25522–25530.
4. Bessimou M, Masrou R. Magnetocaloric effect and magnetic properties of Dy₂CoMnO₆: Monte Carlo study. *Philosophical Magazine*. 2023;103(1): 56–66.

5. El Krimi Y, Masrou R. Cobalt-based full Heusler compounds Co₂FeZ (Z= Al, Si, and Ga): A comprehensive study of competition between XA and L21 atomic ordering with ab initio calculation. *Materials Science and Engineering: B*. 2022;284: 115906.
6. Masrou R, Hlil EK, Hamedoun M, Benyoussef A, Mounkachi O, El Moussaoui H. Ab initio, mean field theory and series expansions calculations study of electronic and magnetic properties of antiferromagnetic MnSe alloys. *Journal of Magnetism and Magnetic Materials*. 2014;361: 197–200.
7. Masrou R, Hlil EK, Hamedoun M, Benyoussef A, Mounkachi O, El Moussaoui H. Ab initio, mean field theory and series expansions calculations study of electronic and magnetic properties of antiferromagnetic MnSe alloys. *Journal of Magnetism and Magnetic Materials*. 2014;361: 197–200.
8. Masrou R, Hlil EK, Hamedoun M, Benyoussef A, Mounkachi O. Electronic and magnetic structures of ferrimagnetic Mn₂Sb compound. *Journal of Magnetism and Magnetic Materials*. 2015;374: 116–119.
9. Masrou R, Hlil EK, Hamedoun M, Benyoussef A, Boutahar A, Lassri H. Antiferromagnetic spintronics of Mn₂Au: An experiment, first principle, mean field and series expansions calculations study. *Journal of Magnetism and Magnetic Materials*. 2015;393: 600–603.
10. Masrou R, Hlil EK, Hamedoun M, Benyoussef A, Mounkachi O. Electronic and magnetic properties of MnAu nanoparticles. *Journal of Magnetism and Magnetic Materials*. 2014;354: 159–162.
11. Baaalla N, Ammari Y, Hlil EK, Masrou R, El Kenz A, Benyoussef A. Study of optical, electrical and photovoltaic properties of CH₃NH₃PbI₃ perovskite: ab initio calculations. *Physica Scripta*. 2020;95(9): 095104.
12. Baaalla N, Ammari Y, Hlil EK, Abid S, Masrou R, Benyoussef A, El Kenz A. The novel material based on strandberg-type hybrid complex (C₆H₁₀N₂)₂ [Co (H₂O) 4P₂Mo₅O₂₃]. 6H₂O: Experimental and simulations investigation on electronic, optical, and magnetocaloric properties. *Ceramics International*. 2021;47(2): 2338–2346.
13. Baaalla N, Hemissi H, Hlil EK, Masrou R, Benyoussef A, El Kenz A. Electronic and optical properties of organic-inorganic (CuII/ReVII)-heterobimetallic L-Arginine complex: Experimental and Computational studies. *Journal of Molecular Structure*. 2021;1246: 131153.
14. Baaalla N, Absike H, Ammari Y, Hlil EK, Masrou R, Benyoussef A, El Kenz A. An extensive investigation of structural, electronic, optical, magnetic, and thermoelectric properties of NaMnAsO₄ cluster by first-principles calculations. *International Journal of Energy Research*. 2022;46(7): 9586–9601.
15. Belyaev FS, Evard ME, Volkov AE. Simulation of the plastic deformation of shape memory alloys considering shear anisotropy on the slip plane. *Materials Physics and Mechanics*. 2023;51(1): 61–67.
16. Breczko T, Barkaline VV, Grechishkin RM, Nelayev VV. Magnetic properties of Ni₂MnGa alloy. *Materials Physics and Mechanics*. 2010;9(1): 53–67.
17. De Groot RA, Mueller FM, PG v. Engen, and KHJ Buschow. *Phys. Rev. Lett*. 1983;50(25): 2024–2027.
18. Julliere M. Tunneling between ferromagnetic films. *Physics letters A*. 1975;54(3): 225–226.
19. Pandey R, Jaffe JE, Kunz AB. Ab initio band-structure calculations for alkaline-earth oxides and sulfides. *Physical Review B*. 1991;43(11): 9228.
20. Yuasa S, Fukushima A, Kubota H, Suzuki Y, Ando K. Giant tunneling magnetoresistance up to 410% at room temperature in fully epitaxial Co/ MgO/ Co magnetic tunnel junctions with bcc Co (001) electrodes. *Applied Physics Letters*. 2006;89(4): 042505.

21. Parkin SS, Kaiser C, Panchula A, Rice PM, Hughes B, Samant M, Yang SH. Giant tunnelling magnetoresistance at room temperature with MgO (100) tunnel barriers. *Nature Materials*. 2004;3(12): 862–867.
22. Hülsen B, Scheffler M, Kratzer P. Thermodynamics of the Heusler alloy $\text{Co}_{2-x}\text{Mn}_{1+x}\text{Si}$: A combined density functional theory and cluster expansion study. *Physical Review B*. 2009;79(9): 094407.
23. Viglin NA, Ustinov VV, Osipov VV. Spin injection maser. *JETP Letters*. 2007;86: 193–196.
24. Klimczuk T, Wang CH, Gofryk K, Ronning F, Winterlik J, Fecher GH, Griveau JC, Colineau E, Felser C, Thompson JD, Safarik DJ. Superconductivity in the Heusler family of intermetallics. *Physical Review B*. 2012;85(17): 174505.
25. Ağduk S, Gökoğlu G. First-principles study of elastic and vibrational properties of Ni_2MnIn magnetic shape memory alloys. *The European Physical Journal B*. 2011;79: 509–514.
26. Uijtewaal MA, Hickel T, Neugebauer J, Gruner ME, Entel P. Understanding the phase transitions of the Ni_2MnGa magnetic shape memory system from first principles. *Physical Review Letters*. 2009;102(3): 035702.
27. Heusler F. Über magnetische manganlegierungen. *Verhandlungen der Deutschen Physikalischen Gesellschaft*. 1903;5: 219.
28. Bradley AJ, Rodgers JW. The crystal structure of the Heusler alloys. *Proceedings of the royal society of london. Series A, Containing Papers of a Mathematical and Physical Character*. 1934;144(852): 340–359.
29. Gencer A, Surucu O, Usanmaz D, Khenata R, Candan A, Surucu G. Equiatomic quaternary Heusler compounds TiVFeZ ($Z = \text{Al, Si, Ge}$): half-metallic ferromagnetic materials. *Journal of Alloys and Compounds*. 2021;883: 160869.
30. Hocine H, Amara K, Khelfaoui F. Half-metallic stability of the Heusler alloys TiZrIrZ ($Z = \text{Al, Ga, and In}$) under volumetric strain and tetragonal deformation. *Applied Physics A*. 2020;126(3): 178.
31. Heusler F, Starck W, Haupt E. Magnetisch-chemische studien. *Verh. Dtsch. Phys. Ges.* 1903;5: 219–232.
32. Heusler O. Crystal structure and the iron magnetism of manganese-aluminium-copper alloys. *Ann. Phys.* 1934;19: 155–201.
33. Hellal T, Bensaïd D, Doumi B, Mohammedi A, Benzoudji F, Azzaz Y, Ameri M. Mn_2YGa ($Y = \text{Ir and Pt}$), a promising shape memory alloy by DFT methods. *Chinese Journal of Physics*. 2017;55(3): 806–812.
34. Kharel P, Huh Y, Shah VR, Li XZ, Al-Aqtash N, Tarawneh K et al. Structural and magnetic properties of $\text{Mn}_{2+\delta}\text{TiSn}$. *Journal of Applied Physics*. 2012;111(7): 07B101.
35. Dahal B, Al Maruf A, Prophet S, Huh Y, Lukashev PV, Kharel P. Electronic, magnetic, and structural properties of Fe_2MnSn Heusler alloy. *AIP Advances*. 2020;10(1): 015118.
36. Keshavarz S, Naghibolashrafi N, Jamer ME, Vinson K, Mazumdar D, Dennis CL, Ratcliff II W, Borchers JA, Gupta A, LeClair P. Fe_2MnGe : A hexagonal Heusler analogue. *Journal of Alloys and Compounds*. 2019;771: 793–802.
37. Sugihara A, Mizukami S, Yamada Y, Koike K, Miyazaki T. High perpendicular magnetic anisotropy in $\text{D}_{22}\text{-Mn}_{3+x}\text{Ge}$ tetragonal Heusler alloy films. *Applied Physics Letters*. 2014;104(13): 132404.
38. Jansen HJ, Freeman AJ. Total-energy full-potential linearized augmented-plane-wave method for bulk solids: Electronic and structural properties of tungsten. *Physical Review B*. 1984;30(2): 561.
39. Kohn W, Sham LJ. Self-consistent equations including exchange and correlation effects. *Physical Review*. 1965;140(4A): A1133.

40. Blaha P, Schwarz K, Medsen GKH, Kvasnicka D, Luitz J. *WIEN2k, An Augmented Plane Wave Plus Local Orbitals Program for Calculating Crystal Properties*. Vienna, Austria: Vienna University Technology; 2001.
41. Schwarz K, Blaha P. Solid state calculations using WIEN2k. *Comput. Mater. Sci.* 2003;28: 259.
42. Kohn W, Sham LJ. Density functional theory. In: *Conference proceedings - Italian Physical Society 1996*. p.561–572.
43. Perdew JP, Burke K, Ernzerhof M. Generalized gradient approximation made simple. *Physical Review Letters*. 1996;77(18): 3865.
44. Perdew JP, Chevary JA, Vosko SH, Jackson KA, Pederson MR, Singh DJ, Fiolhais C. Atoms, molecules, solids, and surfaces: Applications of the generalized gradient approximation for exchange and correlation. *Physical Review B*. 1992;46(11): 6671.
45. Tran F, Blaha P. Accurate band gaps of semiconductors and insulators with a semilocal exchange-correlation potential. *Physical Review Letters*. 2009;102(22): 226401.
46. Murnaghan FD. The compressibility of media under extreme pressures. *Proceedings of the National Academy of Sciences*. 1944;30(9): 244–247.
47. Sayah M, Zeffane S, Mokhtari M, Dahmane F, Zekri L, Khenata R, Zekri N. First-principles investigation of half-metallic ferromagnetism of Fe₂YSn (Y= Mn, Ti and V) Heusler alloys. *Condens. Matter Phys.* 2021;24(2): 23703.
48. Jain VK, Lakshmi N, Jain R, Chandra AR. Electronic Structure, Elastic, Magnetic, and Optical Properties of Fe₂MnZ (Z= Si, Ge, and Sn) Full Heusler Alloys: First-Principle Calculations. *Journal of Superconductivity and Novel Magnetism*. 2019;32: 739–749.
49. Slater JC. The ferromagnetism of nickel. *Physical Review*. 1936;49(7): 537.
50. Pauling L. The nature of the interatomic forces in metals. *Physical Review*. 1938;54(11): 899.
51. Galanakis I, Dederichs PH, Papanikolaou N. Slater-Pauling behavior and origin of the half-metallicity of the full-Heusler alloys. *Physical Review B*. 2002;66(17): 174429.
52. Skaftouros S, Özdoğan K, Şaşıoğlu E, Galanakis I. Search for spin gapless semiconductors: The case of inverse Heusler compounds. *Appl. Phys. Lett.* 2013;102: 022402.
53. Abbassa H, Meskine S, Labdelli A, Kacher S, Belaroussi T, Amrani B. Promising shape memory in NiCoMnZ (Z= Si, Ge and Sn) quaternary Heusler alloy from first principles. *Materials Chemistry and Physics*. 2020;256: 123735.
54. Abbes EH, Abbassa H, Meskine S, Bouhamou I, Boukortt A. First-principles investigation of magneto-electronic properties and band Jahn-Teller effects in NiCoMnSi_{1-x}Al_x quaternary Heusler. *Journal of New Technology and Materials*. 2022;12(2): 62–69.

THE AUTHORS

Bouhamou I.

e-mail: imen.bouhamou.etu@univ-mosta.dz

Abbes C.

e-mail: charef.abbes@univ-mosta.dz

Abbes E.H.

e-mail: habib.abbes.etu@univ-mosta.dz

Abbassa H.

e-mail: abshzm@gmail.com

Boukortt A.

e-mail: boukortt@yahoo.fr

Benbedra A.

e-mail: abdesamed.benbedra@gmail.com